PAPER Special Issue on Heterostructure Microelectronics with TWHM2003

Effect of Heterostructure 2-D Electron Confinement on the Tunability of Resonant Frequencies of Terahertz Plasma-Wave Transistors

Taiichi OTSUJI[†a)], *Regular Member*, Yoshihiro KANAMARU[†*], Hajime KITAMURA[†**], Mitsuru MATSUOKA[†**], *and* Osamu OGAWARA[†], *Nonmembers*

SUMMARY This paper describes an experimental study on resonant properties of the plasma-wave field-effect transistors (PW-FET's). The PW-FET is a new type of the electron devices, which utilizes the plasma resonance effect of highly dense two-dimensional conduction electrons in the FET channel. Frequency tunability of plasma-wave resonance in the terahertz range was experimentally investigated for sub 100-nm gate-length GaAs MESFET's by means of laser-photo-mixing terahertz excitation. The measured results, including the first observation of the third-harmonic resonance in the terahertz range, however, fairly deviate from the ideal characteristics expected for an ideal 2-D confined electron systems. The steady-state electronic charge distribution in the MESFET channel under laser illumination was analyzed to study the effect of insufficient carrier confinement on the frequency tunability. The simulated results support the measured results. It was clarified that an ideal heterostructure 2-D electron confinement is essential to assuring smooth, monotonic frequency tunability of plasma-wave resonance.
key words: *plasma wave, resonance, FET, HEMT, Terahertz, polariton, harmonic resonance*

1. Introduction

Emerging information technologies necessitate further extension of operating frequency bands in electronic systems to beyond terahertz (THz). Conventional semiconductor device technologies, which rely upon real-carrier transport, however, face to the substantial limit of operation in the THz region [1]–[4]. New operating principles should be appreciated to establish novel THz device technology for the real applications [5].

In 1970s, the study on plasma waves in two-dimensional (2-D) electron systems began [6]–[8]. On the basis of those earlier studies, Dyakonov and Shur proposed a new THz electron device utilizing the plasma resonance effect of highly dense 2-D conduction electrons in the FET channel [9]–[12]. We call it hereafter the plasma-wave transistor (PW-FET). The PW-FET does not rely upon the real-carrier transport but upon electronic polarization so that it could break-through the speed limit on conventional electron devices. It also has a great advantage that the resonant frequency can be externally controlled by the gate bias voltage, which results in a possibility of injection-locked frequency-tunable oscillation. This is essential for the applications to the synchronized operation of communications network and/or measurement systems.

So far, various analytical [9]–[17] and some experimental studies [18]–[20] on PW-FET's have been reported. Recently, the gate-bias dependence of the resonant frequency was observed for a sub-100-nm gate GaAs MESFET [20]. Actually, the conduction electrons in the MESFET channel are not well confined along the direction of wafer thickness. Thus the plasma resonance properties should deviate from what is expected for ideally 2-D-confined electron systems. This paper describes further experimental study on its gate-bias dependence including the harmonic resonance in the terahertz rage and discusses the importance of heterostructure 2-D electron confinement for the frequency tunability of plasma-wave resonance.

2. Basic Properties of PW-FET's

Figure 1 schematically explains the principle of operation of the PW-FET's. The PW-FET's are set on a common-source/open-drain configuration. First we assume that the electrons are highly dense and transversely well confined in the channel so that the terahertz radiation can be coherently absorbed via intersubband transitions of conduction electrons. Next, let an $\boldsymbol{E}$ vector of the irradiated electromagnetic wave be parallel to the channel axis (source-drain direction). Under these conditions, the incoming electromagnetic radiation induces an ac voltage at the source side and the plasma waves of electrons are excited. The plasma-wave resonance may occur under the standing wave condition of the fundamental and odd harmonics, which is given by $\lambda = 4L/(2n-1)$ where λ the plasma-wavelength, n an arbitral integer. A coupling with a terahertz radiation might be enhanced using an appropriate antenna structure at the open-drain node.

Under the gradual-channel approximation condition where the DC drain-source bias is sufficiently weak

Manuscript received February 11, 2003.
Manuscript revised March 16, 2003.
[†]The authors are with Graduate School of Computer Science and Systems Engineering, Kyushu Institute of Technology, Iizuka-shi, 820-8502 Japan.
[*]Presently, with Kawasaki Heavy Industry Corp.
[**]Presently, with NTT DoCoMo Kyushu Corp.
a) E-mail: otsuji@ces.kyutech.ac.jp

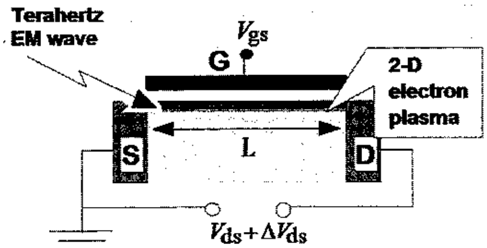

(a) Device cross-section.

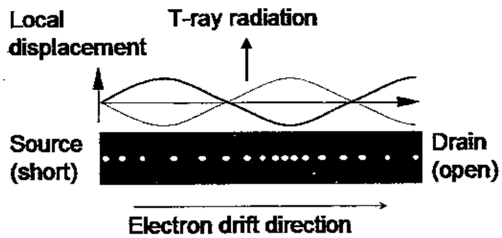

(b) Plasma resonance in the channel.

Fig. 1 Plasma-wave FET.

and the FET is biased only by the gate-to-source voltage V_g, the motion of the plasma waves along with the x axis parallel to the source-to-drain direction can be described by the following hydrodynamic equations [11],

$$-e\frac{\partial V(x)}{\partial x} - m_e\frac{v}{\tau} = m_e\left(\frac{\partial v}{\partial t} + v\frac{\partial v}{\partial x}\right), \quad (1)$$

$$\frac{\partial n_s}{\partial t} + \frac{\partial (n_s v)}{\partial x} = \frac{\partial V(x)}{\partial t} + \frac{\partial (V(x)v)}{\partial x} = 0, \quad (2)$$

where n_s the surface density of conduction electrons, $V(x)$ the gate-to-channel potential at x, m_e the electron effective mass, v the local electron velocity. Equation (1) is the Euler equation. Equation (2) is the continuity equation in which the induced electronic charge $n_e(x)$ is given by the product of the gate-channel potential $V(x)$ and the uniform channel capacitance. By solving (1) and (2) under the boundaries of (i) the common-source/open-drain condition, (ii) terahertz sinusoidal wave absorption $V_a \cos\omega t$ at the source end (far weaker than the gate-source DC bias voltage V_g), the DC component of the source-to-drain voltage induced by the incoming terahertz signal, ΔV, is obtained as follows [11].

$$\frac{\Delta V}{V_a} = \frac{V_a}{4V_g} f(\omega), \quad (3)$$

$$f(\omega) = 1 + \beta - \frac{1 + \beta\cos(2k_0'L)}{\sinh^2(k_0''L) + \cos^2(k_0'L)}, \quad (4)$$

$$\beta = 2\omega\tau/\sqrt{1 + (\omega\tau)^2}, \quad (5)$$

$$k_0' = \frac{\omega}{v_p}\left(\frac{\sqrt{1+\omega^{-2}\tau^{-2}}+1}{2}\right),$$

$$k_0'' = \frac{\omega}{v_p}\left(\frac{\sqrt{1+\omega^{-2}\tau^{-2}}-1}{2}\right), \quad (6)$$

$$v_p = \sqrt{\frac{eV_g}{m_e}} = \sqrt{\frac{edn_s}{\varepsilon m_e}}, \quad (7)$$

where e the electronic charge, d the gate-channel barrier thickness, ε the permittivity of the material. This consequence implies that the plasma resonance effect modulates the DC drain-source potential. Therefore, you may indirectly measure the resonant intensity by monitoring the DC modulation component ΔV_{ds} the frequency and intensity of the plasma-wave resonance can be evaluated by (3)–(7). We discuss, hereafter, the plasma resonance characteristics using the $f(\omega)$ value.

In (4), the parameter $k_0'L$ determines the resonant frequency while $k_0''L$ gives the damping or attenuation effect. Here, the plasma relaxation time τ, a variable of k_0' and k_0'', is defined as $1/\tau = 1/\tau_m + 1/\tau_\nu$, where τ_m the mean electron collision time with phonons and impurities (due to external friction) and τ_ν the damping time due to the viscosity of the electron fluid (due to internal friction caused by electron-electron scattering). The coherence length of the plasma wave is thus defined as $v_p\tau$. The dimensionless parameter $v_p\tau/L$ gives the resonant intensity or the quality factor [11]. The condition, $v_p\tau/L = 1$, therefore, gives rise to the break-even point for the resonance where the plasma coherence length corresponds to the gate length.

When $\omega\tau \gg 1$, $k_0'L \approx \omega L/v_p$ and $k_0''L \approx L/(2v_p\tau)$. Thus, the fundamental plasma resonant frequency ω_0 is given by $\pi v_p/(2L)$. Since v_p is a function of V_g as seen in (7), the gate bias voltage can externally control the resonant frequency. This is an essential function for the applications to the synchronized operation of communications network and/or measurement systems.

The dependence of the plasma-resonance characteristics on gate length L was analyzed for GaAs MESFET's at 300 K. The DC gate bias voltage V_g was set at 1.0 V while the DC drain-to-source bias was set at close to 0 V. The corresponding fundamental resonant frequency, which is simply given by $v_p/4L$, stays 0.7 to 11.7 THz. For $0.03\,\mu\text{m} < L < 0.1\,\mu\text{m}$, the resonant intensity $v_p\tau/L$ stays in between 3 and 6, which sufficiently falls in the resonance-intensive condition of $v_p\tau/L > 1$. Simulated results indicate that sub-100-nm gate-length GaAs-based FET's can exhibit an intensive plasma resonant oscillation in the terahertz range [17].

The plasma resonance properties were simulated for 80-nm gate-length GaAs MESFET's (equivalent to the sample for experiments) at 300 K. As mentioned above, the plasma relaxation time τ ($1/\tau = 1/\tau_m + 1/\tau_\nu$) is the key parameter. τ_m the mean electron collision time with phonons and impurities was determined from the electron mobility μ ($= 5500\,\text{cm}^2/\text{Vs}$) and the electron effective mass m ($= 0.067m_0$) as $\tau_m = m\mu/e$ [17]. τ_ν the damping time due to the viscosity (electron-electron scattering) of the electron fluid was given by $(\nu k^2)^{-1}$, where k is the wave number and ν the electron fluid viscosity $\nu \approx \hbar/m$, where $\hbar$ the Plank constant [9], [17]. The upper limit on the gate bias voltage was set at 1.0 V taking device breakdown into account while the drain bias voltage was set at close to zero so as to make a gradual-channel approximation. It is noted that an ideal 2-D electron confinement was assumed even for the MESFET's in order to support the above simplified calculation. The simulated gate-bias dependence of the plasma resonant intensity is plotted in Fig. 2 at excitation frequencies of 1.5 THz and its third harmonic 4.5THz in (a) and 2.5 THz and its third harmonic 7.5 THz in (b). The vertical axis is calculated by $\Delta \bar{V}_{ds} V_g$ corresponding to the plasma resonant intensity [11]. For all the excitation conditions, resonant peaks are clearly seen.

Figure 3 plots the simulated resonant frequencies (f_r) versus the gate bias voltage V_g. Resonance-intensive regions ($v_p \tau / L \geq 1$) are specified with thick lines. For the fundamental and third harmonic resonance, a very wide frequency tunability of 1.5 THz $\leq f_r \leq$ 3.5 THz and that of 4.5 THz $\leq f_r \leq$ 11.0 THz are obtained, respectively. For the third harmonic resonance, the resonant intensity drastically decreases. This is because the electron-electron scattering increases in proportion to the square of the resonant frequency. Actual electron distribution in the channel (not well confined along the vertical direction) may cause deviation of the resonant properties from those simulated results.

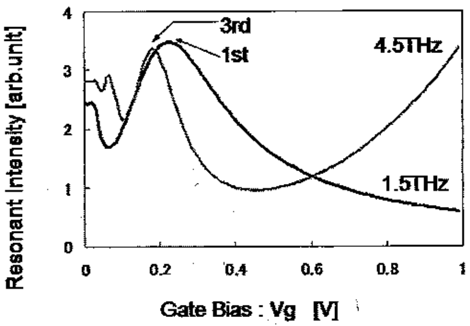

(a) Excitation frequencies of 1.5 and 4.5 THz.

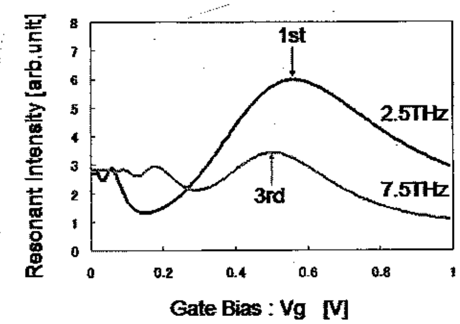

(b) Excitation frequencies of 2.5 and 7.5 THz.

Fig. 2 Simulated plasma resonant intensity vs. gate bias voltage for 80-nm gate-length GaAs MESFET at 300 K.

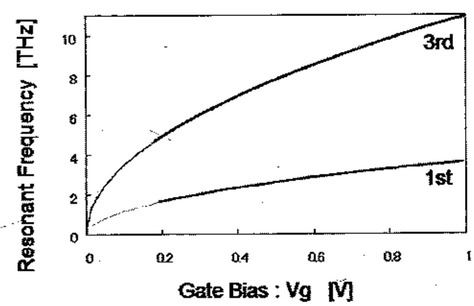

Fig. 3 Simulated fundamental and third harmonic resonant frequencies vs. gate bias voltage for 80-nm gate-length GaAs MESFET at 300 K. The gate-bias voltage is set at 0.5 V. The portions with thicker lines are resonance-intensive region.

3. Terahertz Plasma-Wave Excitation in PW-FET's

One of the major concerns of PW-FET's is the frequency tunability. The dependence of the resonant frequency of PW-FET's on V_g is to be observed for an 80-nm-gate GaAs MESFET. To conduct this experiment, plasma-wave excitation in the terahertz range is an essential function and is performed by means of polariton-plasmon interaction, i.e. photon-phonon coupling and coherent phonon-plasmon interaction [17], [20]. Hirakawa et al. experimentally suggested that the photon with $< E_g$ coherently excites the plasmon via polariton [21]. Also, Gu et al. observed the terahertz electromagnetic wave radiation from LO-phonon plasmon coupling modes in InSb film [22]. Three mechanisms of the coherent LO-phonon excitation are known: (i) impulsive stimulated Raman scattering (ISRS) [23], (ii) displacive excitation of coherent phonon (DECS) [24], and (iii) instantaneous screening of surface potential bending (ISSPB) [25]. ISRS requires photon energy slightly less than E_g while DECS and ISSPB require photon energy lager than E_g. These prior works should support the mean of terahertz plasma-wave excitation taken in this experiment. It is also thought for GaAs materials that the photon energy of far less than E_g could excite the coherent LO phonon due to the existence of the deep trap centers [27], [28].

3.1 Experimental Setup and Sample Preparation

Experimental setup is shown in Fig. 4. A pair of wavelength-tunable continuous-wave (CW) laser sources having a 100-nm band around 1550 nm was prepared for. The Terahertz excitation was performed by using a pair of C-band tunable CW laser sources in a manner of difference-frequency (Δf) generation via polariton-plasmon interaction [20]. The resonant intensity was estimated by monitoring the DC modulation component ΔV_{ds} of the source-drain potential ($O(100\,\mu\text{V})$). The gate-bias (V_g) dependence of ΔV_{ds} was precisely measured by using a lock-in amplifier.

The sample under measurement was an 80-nm

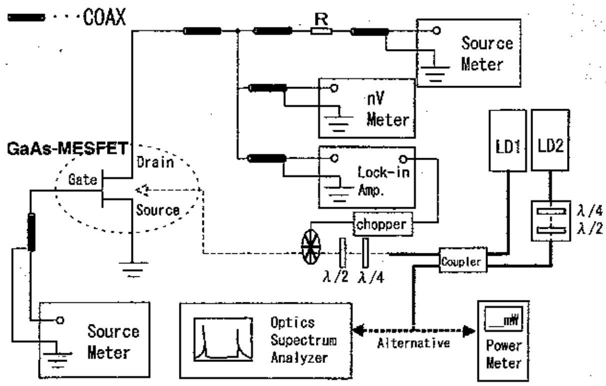

Fig. 4 Experimental setup: LD: laser diode unit, COAX: coaxial cables, R: load resistor.

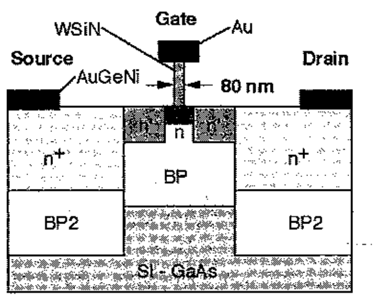

(a) Cross sectional view.

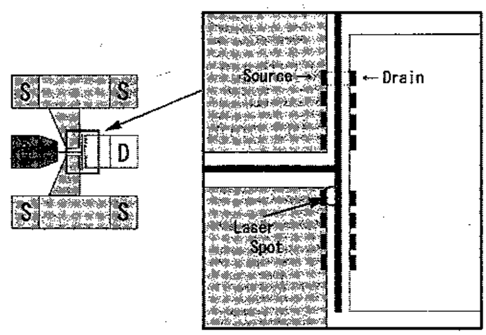

(b) Pad layout and probing geometry.

Fig. 5 Device structure of GaAs MESFET.

gate-length GaAs MESFET [26]. The gate width is 100 μm (12.5 μm × 8 sections). Its cross sectional view is shown in Fig. 5(a). The two-step buried p-layer (BP and BP2) lightly-doped drain (LDD) structure is adopted, which is effective in suppressing the short channel effects. The gate electrode is formed with a T-shaped Au/WSiN structure. Offsets (Ln′-Lg), which separate the gate electrode from the n′ layers, also help reduce the gate parasitic capacitance. Typical DC/AC characteristics: the threshold voltage V_{th}, the transconductance G_m, the current-gain cutoff frequency f_T, and the maximum oscillation frequency $f_{\max}$, are −1.0 V, 400 mS/mm, 100 GHz, and 110 GHz, respectively. The sample was measured on wafer under a common-source/near-open-drain condition with a load resistor of 1 kΩ. The photomixed laser beam

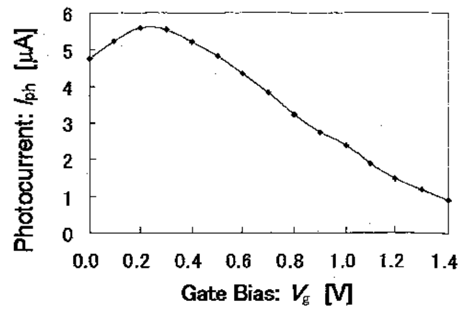

Fig. 6 Measured photoexcited current vs. gate bias V_g. The drain-to-source bias V_{ds} was set at +0.2 V. The incident laser beam is a 1550-nm wavelength, CW source with an average power of 3 mW.

was linearly polarized along the channel axis and illuminated onto one section of the channel from the backside as shown in Fig. 5(b). For this purpose, the backside of the wafer was chemically polished to make an optical flat surface.

3.2 Experimental Results

3.2.1 Photoresponse of GaAs MESFET's

In general, the semi-insulating GaAs material is transparent to the photon in the 1550-nm range. Thus, virtual carrier excitation using polariton-plasmon interaction by photomixing the 1550-nm sources with THz difference-frequency component would be a reasonable way for plasma excitation [17]. However, because of the deep trap centers produced by Cr and O doping for defect compensation [27], [28], weak but steady photocurrent I_{ph} was generated under the laser illuminations. I_{ph}-V_g characteristics were measured at the channel area. The V_{ds} was set at +0.2 V. Typical result is shown in Fig. 6. At lower V_g region where the gate-channel Schottky diode is strongly reverse-biased, the depleted-region is enlarged and photoexcited electrons drift along the potential gradient to the channel with large velocity, yielding large photocurrent (on the order of 10 μA). With increasing the V_g, the photocurrent monotonically decreased, reflecting the bias dependence of the Schottky diode.

The I_{ph} profile along the channel axis was also measured. The result, as shown in Fig. 7, indicates that the photocurrent exhibits a local minimum at the very center of the channel and rapidly increases with leaving the channel region for both sides of the source and drain. As shown in Fig. 8, the photoexcitation processes via those trap centers are considered to occur at the p-n junctions of the buried p-layer and upper n, n′, and n^+ layers as well as at the gate-channel Schottky junction. From the channel region (n) to the outer regions (n′ and further n^+ region), both the area and the potential gradient of the p-n junction increase. The measured I_{ph} profile well reflects this physical aspect

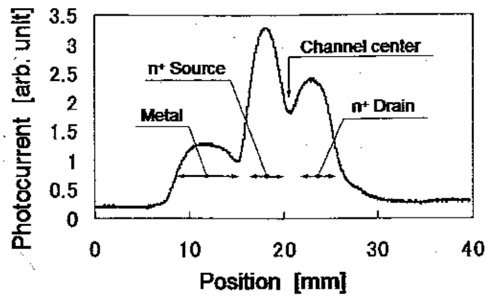

Fig. 7 Measured photocurrent profile along the channel axis (source-to-drain) direction.

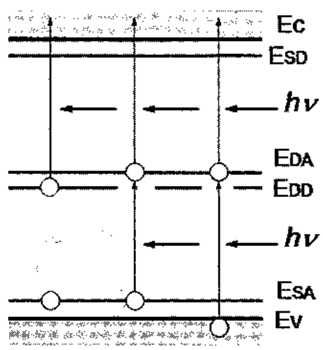

Fig. 8 Possible photoexcitation processes via deep trap centers in GaAs.

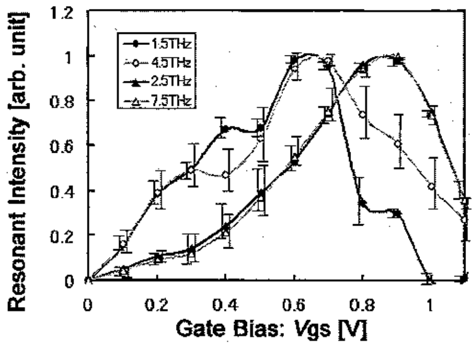

Fig. 9 Measured plasma-resonant intensity vs. gate bias V_g.

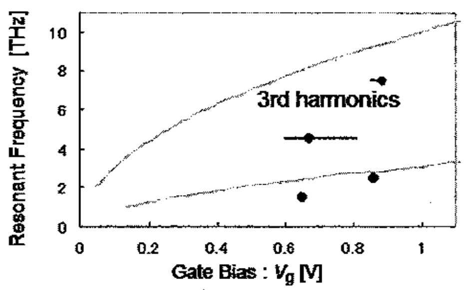

Fig. 10 Measured plasma-resonant frequencies vs. gate bias V_g. The shaded lines are simulated results under the condition of ideal 2-D electron confinement.

of photoexcitation processes. This leads to an important consequence that accurate beam positioning can be performed by searching for the local minimal I_{ph} point.

3.2.2 Plasma Resonance Properties

For terahertz plasma-wave excitation, the difference frequencies Δf were set at 1.5 and 2.5 THz, and their third harmonics: 4.5 and 7.5 THz. In order to discriminate the effect of the plasma resonance from the background (mainly due to undesirable photoexcited real carriers as mentioned above), the DC drain-source voltages (initially biased at 0.2 V) under a zero-Δf condition was also measured and subtracted from those under the non-zero-Δf condition, obtaining the DC drain-source modulation component ΔV_{ds}.

Measured results for plasma resonant intensity versus V_g are plotted in Fig. 9. Due to residual uncertainty on the absolute value of the resonant intensity (mainly caused by the fluctuation of the incident laser power), the resonant intensity was normalized by the peak intensity on each curve. The results indicate the occurrence of plasma resonance at the peak point on each curve. The V_g value at the resonance point, V_{g-R}, for Δf_r of 1.5 THz (2.5 THz) almost coincides with that for Δf_r of 4.5 THz (7.5 THz). This implies, as is analytically derived, that the third harmonic resonance was observed for Δf_r of 4.5 and 7.5 THz. This is the first observation of the third harmonic resonance for PW-FET's in the THz range.

Figure 10 plots the resonant frequency f_r versus the gate bias V_g. The shaded lines are the simulated results for an ideal 2-D electron confinement in heterostructures where f_r monotonically increases in proportion to $\sqrt{V_{gs}}$, assuring smooth frequency tunability. The measured results, however, fairly deviate from the ideal characteristics at lower V_g region. The f_r rapidly increases with slight increase in V_g of around 0.7 V, degrading the frequency tunability.

4. Discussion

4.1 Quality Factor of the Plasma Resonance

Seeing more precisely in Fig. 9, all the resonant curves show much broader aspects (lower quality factors) than those for the first-order simple analytical estimation as shown in Figs. 3(a) and (b). The following two factors are considered for this reason: insufficient electron confinement along with the directions (i) perpendicular to the channel and (ii) longitudinal to the channel. Due to the nature of the MESFET structure, insufficient electron confinement makes a certain distribution of the electron density along with the channel thickness direction. This may directly broaden the resonant curve. On the other hand, carrier confinement along with the channel seems to be also insufficient. This is because the channel boundaries (the source and drain ends) are defined by the fraction of the electron density between inside and outsides of the channel (formed with the n^+ ohmic contact regions), and are somewhat lossy.

4.2 Carrier Distribution in MESFET Channel under Weak Photoexcitation

The cause of such poor frequency tunability (as is seen in Fig. 10) is considered. As mentioned in Sect. 2, when assuming both the density of electrons and the motive force to the plasma wave are directly given by the gate-to-source potential V_g, the plasma-wave velocity v_p, then the resonant frequency f_r, is proportional to $\sqrt{V_{gs}}$ (see Eq. (7)). This is an ideal case for heterostructure 2-D electron systems. In an actual sample of MESFET's, however, we must consider the carrier distribution along with the vertical direction, which is originated from the nature of the MESFET's structure. Since the effective channel thickness d of the sample (MESFET's) cannot be ignored and varies with V_g and photoexcitation, the increase in electronic charge (induced by V_g and photoexcitation) in the channel does not simply reflect the increase in the surface density of electrons n_s. Therefore, in order to obtain an actual v_p or f_r, the real carrier distribution and then the effective density of electrons that gives the effective motive force to the plasma waves should be calculated.

The band diagrams of a depletion-type MESFET are shown in Fig. 11. The horizontal axis takes the normal direction to the surface; the left side corresponds to the gate metal and the right side corresponds to the buried p-layer. The effective channel region is defined as the central region with the thickness d in between the depleted layers W_1 and W_3 in the Schottky and p-n junctions. The effective channel thickness d and the distribution of conduction electrons are modulated by the gate bias V_g and photoexcitation.

Under a weak, constant photoexcitation condition with photon energy of less than the band gap energy, it is reasonable that the band structure (potential gradient) is dominantly determined by V_g and less affected by the photoexcitation. In this case, the total carrier distribution $n_{tot}(x, V_g)$ is approximated by the sum of the independent two processes: (i) carrier distribution $n_{non}(x, V_g)$ under a V_g condition without photoillumination, and (ii) photoexcited carrier distribution $n_{ph}(x, V_g)$.

$$n_{tot}(x, V_g) = n_{non}(x, V_g) + n_{ph}(x, V_g) \tag{8}$$

Assuming an actual physical parameters for the channel, the carrier distribution without photoillumination, $n_{non}(x, V_g)$, were calculated as

$$n_{non}(x, V_g) = 2\left(\frac{2\pi m_e k_B T}{h^2}\right)^{3/2} \cdot \frac{1}{1+\exp\left(\dfrac{E_c(x, V_g) - E_F}{k_B T}\right)}, \tag{9}$$

where m_e the effective mass of a conduction electron, k_B the Boltzmann constant, T the temperature, $E_c(x, V_g)$ the potential at the bottom of the conduction band, and E_F the Fermi energy.

On the other hand, steady-state distribution of photoexcited carriers, $n_{ph}(x, V_g)$, was analyzed by solving the rate equation:

$$\frac{\partial n_{ph}}{\partial t} = G - \frac{n_{ph}}{\tau} + D_e \frac{\partial^2 n_{ph}}{\partial x^2} + \mu_e n_{ph} \frac{\partial E}{\partial x} = 0, \tag{10}$$

where G the carrier generation rate, τ the recombination lifetime, D_e the electron diffusion coefficient, μ_e the electron mobility, E the electric field due to the potential gradient at the bottom of the conduction band. The parameters G and τ were set at optimal values so as to support the measured photocurrent and the reported data for deep trap centers due to Cr and O doping. The parameters D_e, μ_e were set at the standard values for GaAs materials including the velocity overshoot effects.

Calculated $n_{non}(x, V_g)$, $n_{ph}(x, V_g)$ and $n_{tot}(x, V_g)$ are plotted in Figs. 12(a), (b), and (c). The gate bias voltage V_g (offset from the threshold voltage) was set at +0.2, +0.5, +0.7, +1.0, and +1.2 V. With increase in V_g, $n_{non}(x, V_g)$ increases, and its distribution spreads toward the top surface (see Fig. 12(a)). This is a normal dependence for MESFET's. On the other hand, $n_{ph}(x, V_g)$ has larger and wider distribution at lower V_g, which is due to the wider depleted layer in the reverse-biased Schottky junction (see Fig. 12(b)). As a consequence, the total carrier density $n_{tot}(x, V_g)$ takes non-monotonic dependence on V_g as shown in Fig. 12(c). An effective channel thickness d can be defined as the region where $n_{tot}(x, V_g)$ is higher than a certain level. Here we set the border at the density of conduction electrons in the channel under the thermally equilibrium condition at room temperature: $1.3 \times 10^{21}\,\mathrm{m}^{-3}$. As is seen in the inset in Fig. 12(c), $n_{ph}(x, V_g)$ makes d larger in lower V_g region so that d may varies non-monotonically with V_g.

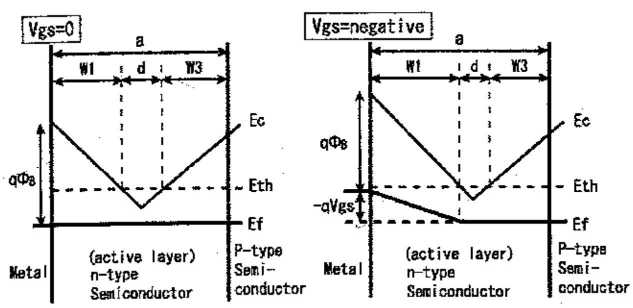

(a) Non-biased condition. (b) Reverse-biased condition.

Fig. 11 Band diagrams of a depletion-type MESFET.

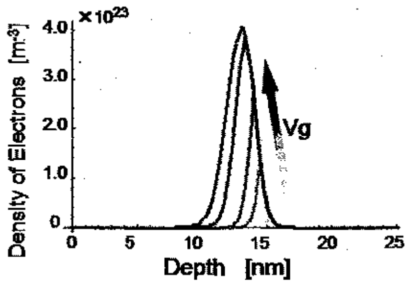

(a) $n_{non}(x)$ without photoillumination.

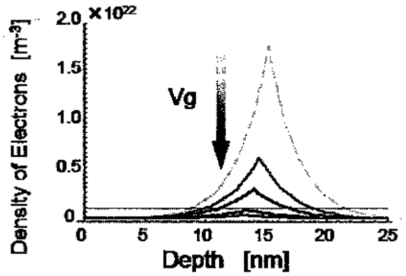

(b) $n_{ph}(x)$ under photoillumination.

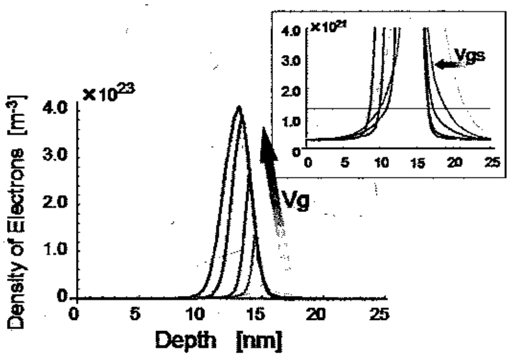

(c) Total density of electrons $n_{tot}(x)$.

Fig. 12 Calcurated carrier distribution in the channel. The parameter, gate-to-source bias voltage V_g (offset value from the threshold voltage), is at +0.2, +0.5, +0.7, +1.0, and +1.2 V.

4.3 Effect of 2-D Carrier Confinement on Frequency Tunability

The mean surface electron density, $\overline{n_{se}(V_g)}$, was calculated as a function of photoexcited carriers and V_g.

$$\overline{n_{se}(V_g)} = \left[\overline{n_{tot}(x, V_g)}\right]^{2/3} = \left[\frac{1}{d}\int_{w1}^{w2} n_{tot}(x, V_g)dx\right]^{2/3} \qquad (11)$$

Then, by substituting n_{se} with $\overline{n_{se}}$ in (7), the V_g dependence of f_r was obtained as shown in Fig. 13 with solid lines. Such an undesirable nonlinear dependence is caused by (i) the finite carrier distribution along the channel thickness decreasing the effective carrier density and (ii) the photoexcited electrons (generated via deep trap centers) at the gate-to-channel depletion region drifting along the potential gradient to increase the effective channel thickness (decrease the depletion layer thickness). It is also noted that insufficient 2-D carrier confinement degrades the quality factor of the plasma resonance because a different density of carriers makes a different resonant frequency. As Crowne reported in [14], [15], the other two important factors that weaken the resonant intensity and coherency should also be considered: 1) the Doppler effect generating up- and down-shifted frequency components [14], 2) non-uniformity of the channel charge density [15]. From the above discussion, it was clarified that an ideal heterostructure 2-D electron confinement is essential to assuring smooth, monotonic frequency tunability of plasma-wave resonance.

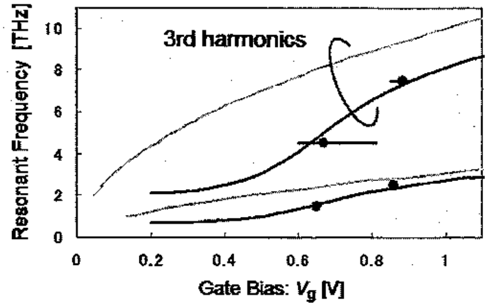

Fig. 13 Simulated plasma-resonant frequencies vs. gate bias V_g. The solid lines are for the results taking carrier distributions and an effective channel thickness into account.

5. Conclusion

Frequency tunability of plasma-wave resonance in the terahertz range was experimentally investigated for sub 100-nm gate-length GaAs MESFET's by means of laser-photo-mixing terahertz excitation. The measured results, including the first observation of the third-harmonic resonance in the terahertz range, however, fairly deviated from the ideal characteristics expected for an ideal 2-D confined electron systems. The steady-state electronic charge distribution in the MESFET channel under laser illumination was analyzed to study the effect of insufficient carrier confinement on the frequency tunability. The simulated results well explained the measured results. It was clarified that an ideal heterostructure 2-D electron confinement is essential to assuring smooth, monotonic frequency tunability of plasma-wave resonance.

Acknowledgements

The authors would like to acknowledge Dr. Hirohiko Sugahara and Dr. Koichi Narahara at NTT Laboratories for their valuable discussion and providing the GaAs MESFET wafer samples. This work is supported in part by Grant-in-Aid for Scientific Research B (#13450147) and for Exploratory Research (#13875069) from the Ministry of Education, Science

Sports and Culture, Japan.

References

[1] M. Rodwell, Q. Lee, D. Mensa, J. Guthrie, Y. Betser, S.C. Martin, R.P. Smith, J. Jaganathan, T. Mathew, P. Krishnan, C. Serhan, and S. Long, "Heterojunction bipolar transistors with greater than 1 THz extrapolated power-gain cutoff frequencies," Proc. IEEE Int. Conf. Terahertz Electron., pp.120–123, Nara, Nov. 1999.

[2] Y. Yamashita, A. Endoh, K. Shinohara, K. Hikosaka, T. Matsui, S. Hiyamizu, and T. Mimura, "Pseudomorphic $In_{0.52}Al_{0.48}As/In_{0.7}Ga_{0.3}As$ MESFETs with an ultrahigh f_T of 562 GHz," IEEE Electron Device Lett., vol.23, no.10, pp.573–575, 2002.

[3] B. Jagannathan, J.-S. Rieh, and G. Freeman, "Scaling towards 300 GHz f_T/f_{MAX} SiGe transistors," Dig. 5th Topical Workshop on Heterostructure Microelectron. (TWHM 2003), pp.112–113, Okinawa, Jan. 2003.

[4] T. Otsuji, "Present and future of high-speed compound semiconductor IC's," Int. J. High Speed Electron. Syst., vol.13, no.1, pp.1–25, 2003.

[5] Proc. IEEE Int. Conf. Terahertz Electron., Nara, 1999.

[6] M. Nakayama, "Theory of surface waves coupled to surface carriers," J. Phys. Soc. Jap., vol.36, no.2, pp.393–398, 1974.

[7] S.J. Allen, Jr., D.C. Tsui, and R.A. Logan, "Observation of the two-dimensional plasmon in silicon inversion layers," Phys. Rev. Lett., vol.38, no.17, pp.980–983, 1977.

[8] D.C. Tsui, E. Gornik, and R.A. Logan, "Far infrared emission from plasma oscillations of Si inversion layers," Solid State Comm., vol.35, no.11, pp.875–877, 1980.

[9] M. Dyakonov and M. Shur, "Shallow water analogy for a ballistic field effect transistor: New mechanism of plasma wave generation by dc current," Phys. Rev. Lett., vol.71, no.15, pp.2465–2468, Oct. 1993.

[10] M. Dyakonov and M. Shur, "Choking of electron flow—A mechanism of current saturation in field effect transistors," Phys. Rev. B, vol.51, no.20, pp.14341–14345, 1995.

[11] M. Dyakonov and M. Shur, "Detection, mixing, and frequency multiplication of terahertz radiation by two-dimensional electronic fluid," IEEE Trans. Electron Devices, vol.43, no.3, pp.380–387, March 1996.

[12] M.S. Shur and M. Dyakonov, "Two-dimensional electrons in field effect transistors," Int. J. High Speed Electron. Syst., vol.9, no.1, pp.65–99, 1998.

[13] M.V. Cheremisin, M.I. Dyakonov, M.S. Shur, and G. Samsonidze, "Influence of electron scattering on current instability in field effect transistors," Solid-State Electron., vol.42, no.9, pp.1737–1742, 1998.

[14] F.J. Crowne, "Contact boundary conditions and the Dyakonov-Shur instability in high electron mobility transistors," J. Appl. Phys., vol.82, no.3, pp.1242–1254, 1997.

[15] F.J. Crowne, "Dyakonov-Shur plasma excitations in the channel of a real high-electron mobility transistor," J. Appl. Phys., vol.87, no.11, pp.8056–8063, 2000.

[16] T. Otsuji, S. Nakae, and H. Kitamura, "Plasma-wave transistors with virtual carrier excitation using polariton-plasmon coupling for terahertz applications," Dig. Topical Workshop on Heterostructure Microelectron. (TWHM 2000), pp.58–59, Kyoto, Aug. 2000.

[17] T. Otsuji, S. Nakae, and H. Kitamura, "Numerical analysis for resonance properties of plasma-wave field-effect transistors and their terahertz applications to smart photonic network systems," IEICE Trans. Electron., vol.E84-C, no.10, pp.1470–1476, Oct. 2001.

[18] J.-Q. Lü, M. Shur, J.L. Hesler, L. Sun, and R. Weikle, "Terahertz detector utilizing two-dimensional electronic fluid," IEEE Electron Device Lett., vol.19, no.10, pp.373–375, Oct. 1998.

[19] M. Shur and J.-Q. Lü, "Terahertz sources and detectors using two-dimensional electronic fluid in high-electron mobility transistors," IEEE Trans. Microw. Theory Tech., vol.48, no.4, pp.750–756, 2000.

[20] T. Otsuji, Y. Kanamaru, H. Kitamura, and S. Nakae, "Terahertz plasma-wave excitation in 80-nm gate-length GaAs MESFET by photomixing long-wavelength CW laser sources," Dig. 59th Annual Dev. Res. Conf., pp.97–98, Notre Dame, IN, June 2001.

[21] K. Hirakawa, N. Sekine, M. Vosseburger, P. Haring-Boliver, and H. Kurz, "Crossover from impulsive to step-function-like excitation of two-dimensional plasmons in AlGaAs/GaAs quantum wells by femtosecond laser pulses," Proc. IEEE Int. Conf. Terahertz Electron., pp.109–111, Nara, Nov. 1999.

[22] P. Gu, M. Tani, K. Sakai, and T.-R. Yang, "THz radiation from LO-phonon-plasmon coupling modes in InSb film," Proc. IEEE Int. Conf. Terahertz Electron., pp.181–184, Nara, Nov. 1999.

[23] Y.-X. Yan and K.A. Nelson, "Impulsive stimulated light scattering. I. General theory," J. Chem. Phys., vol.87, no.11, pp.6240–6256, 1987.

[24] H.J. Zeiger, J. Vidal, T.K. Cheng, E.P. Ippen, G. Dresselhaus, and M.S. Dresselhaus, "Theory for displacive excitation of coherent phonons," Phys. Rev. B, vol.45, pp.768–778, 1992.

[25] G.C. Cho, W. Kütt, and H. Kurz, "Subpicosecond time-resolved coherent-phonon oscillations in GaAs," Phys. Rev. Lett., vol.65, pp.764–766, 1990.

[26] M. Tokumitsu, M. Hirano, T. Otsuji, S. Yamaguchi, and K. Yamasaki, "A 0.1-μm self-aligned-gate GaAs MESFET with multilayer interconnection structure for ultra-high-speed IC's," Tech. Dig. IEEE Int. Electron Dev. Meeting, (IEDM 1996), pp.211–214, 1996.

[27] G.M. Martin, A. Mitonneau, and A. Mircea, "Electron traps in bulk and epitaxial GaAs crystals," Electron. Lett., vol.13, no.7, pp.191–193, 1977.

[28] A. Mitonneau, G.M. Martin, and A. Mircea, "Hole traps in bulk and epitaxial GaAs crystals," Electron. Lett., vol.13, no.22, pp.666–668, 1977.

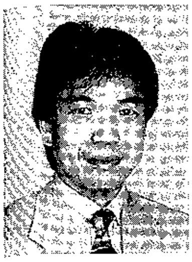

Taiichi Otsuji received the B.S. and M.S. degrees in electronic engineering from Kyushu Institute of Technology, Fukuoka, Japan, in 1982 and 1984, respectively, and the Ph.D. degree in electronic engineering from Tokyo Institute of Technology, Tokyo, Japan, in 1994. From 1984 through 1999, he worked for NTT Laboratories, Kanagawa, Japan, where he developed high-speed LSI test systems, ultra-high-speed optical communication ICs and ultrafast optoelectronic measurement systems. In April 1999, he joined the Department of Control Engineering and Science, Faculty of Computer Science and Systems Engineering, Kyushu Institute of Technology, Fukuoka, Japan, where he is currently a professor. His current research interest includes terahertz electronics, ultrafast optoelectronic measurement, high-speed IC design, and optical communications technologies. He has been authored and co-authored more than 100 peer-reviewed journal papers and conference proceedings, and holds eight Japanese and three US patents. Dr. Otsuji is the recipient of the Outstanding Paper Award of the 1997 IEEE GaAs IC Symposium. He is a member of the IEEE, OSA, and the Japan Society of Applied Physics.

Yoshihiro Kanamaru was bone in Fukuoka, Japan, in 1978. He received the B.S. and M.S. degrees in information engineering from Kyushu Institute of Technology, Fukuoka, Japan, in 2001 and 2003, respectively. He is presently with Kawasaki Heavy Industry Corp., Kobe, Japan.

Hajime Kitamura was bone in Fukuoka, Japan, in 1977. He received the B.S. and M.S. degrees in information engineering from Kyushu Institute of Technology, Fukuoka, Japan, in 2000 and 2002, respectively. He is presently with NTT DoCoMo Kyushu Corp., Ohita, Japan. He is a member of the Japan Society of Applied Physics.

Mitsuru Matsuoka was bone in Fukuoka, Japan, in 1978. He received the B.S. and M.S. degrees in information engineering from Kyushu Institute of Technology, Fukuoka, Japan, in 2001 and 2003, respectively. He is presently with NTT DoCoMo Kyushu Corp., Kumamoto, Japan. He is a member of the Japan Society of Applied Physics.

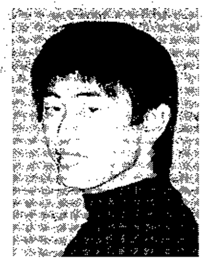

Osamu Ogawara was bone in Okayama Japan, in 1979. He graduated from the Department of Control Engineering and Science, Faculty of Computer Science and Systems Engineering, Kyushu Institute of Technology in 2002. He is presently with the Graduate School of Computer Science and Systems Engineering, Kyushu Institute of Technology, and working toward the M.E. degree.